Carbon Capture Science & Technology 12 (2024) 100202

Contents lists available at ScienceDirect

Carbon Capture Science & Technology

journal homepage: www.elsevier.com/locate/ccst

Full Length Article

Exergy analysis in intensification of sorption-enhanced steam methane reforming for clean hydrogen production: Comparative study and efficiency optimisation

William George Davies[a], Shervan Babamohammadi[a], Yongliang Yan[b], Peter T. Clough[c], Salman Masoudi Soltani[a,*]

[a] Department of Chemical Engineering, Brunel University London, Uxbridge UB8 3PH, UK
[b] School of Engineering, Newcastle University, Newcastle Upon Tyne NE1 7RU, UK
[c] Energy and Sustainability Theme, Cranfield University, Cranfield, Bedfordshire MK43 0AL, UK

ARTICLE INFO

Keywords:
Exergy analysis
Hydrogen
Sorption-enhanced steam methane reforming
Chemical-looping combustion
Carbon capture

ABSTRACT

Hydrogen has a key role to play in decarbonising industry and other sectors of society. It is important to develop low-carbon hydrogen production technologies that are cost-effective and energy-efficient. Sorption-enhanced steam methane reforming (SE-SMR) is a developing low-carbon (blue) hydrogen production process, which enables combined hydrogen production and carbon capture. Despite a number of key benefits, the process is yet to be fully realised in terms of efficiency. In this work, a sorption-enhanced steam methane reforming process has been intensified *via* exergy analysis. Assessing the exergy efficiency of these processes is key to ensuring the effective deployment of low-carbon hydrogen production technologies. An exergy analysis was performed on an SE-SMR process and was then subsequently used to incorporate process improvements, developing a process that has, theoretically, an extremely high CO_2 capture rate of nearly 100 %, whilst simultaneously demonstrating a high exergy efficiency (77.58 %), showcasing the potential of blue hydrogen as an effective tool to ensure decarbonisation, in an energy-efficient manner.

1. Introduction

1.1. Research background

Reduction of greenhouse gas (GHG) emissions by 2050 is of ever-increasing importance. Increasing GHG emissions across the previous two centuries has led to a changing climate that has seen increasing temperatures, rising sea levels and extreme weather events (Guardian, 2023). Climate change is a grand challenge faced within our society that requires significant investment from key stakeholders such as policymakers, scientists and people within industry to ensure that a transition away from GHG is done in a fair and just manner (Wang and Lo, 2021). A major shift in policy has occurred within the last decade since The Paris Agreement, in which governments have developed policy frameworks which further commit countries to ensure only 2 °C of temperature rise by 2050 in comparison to pre-industrial levels (IEA, 2021). Within the UK, this has been outlined by the Build Back Greener and the development of low-carbon industrial clusters across the country (DESNZ and BEIS, 2021a).

Low-carbon hydrogen is an integral part of transitioning away from an economy previously centred on the extraction of oil and gas as well as the release of subsequent CO_2 into the atmosphere (DESNZ and BEIS 2021b). Hydrogen has been identified as a clean-energy carrier, capable of decarbonising a vast range of industries such as maritime (Fu et al., 2023), transport (Singh et al., 2015) and steel (Marocco et al., 2023). There has been increasing interest in the production of low-carbon hydrogen as currently, the main methods of hydrogen production involve the release of significant quantities of CO_2 emissions (i.e. the conventional grey and black hydrogen production) (IEA, 2022). There are several hydrogen production methods which are often referred to as the “colours of hydrogen”. Three of these methods known as blue, green and turquoise hydrogen have been identified as key to developing low-carbon hydrogen production process. Blue hydrogen involves the capture and storage of CO_2 emissions (CCS) during hydrogen production from fossil fuels, whereas green hydrogen production involves the splitting of water *via* electrolysis from ideally renewable electricity (George et al., 2022). Turquoise hydrogen involves the pyrolysis of methane to produce two-high value products: hydrogen and carbon

* Corresponding author.
E-mail address: Salman.MasoudiSoltani@brunel.ac.uk (S. Masoudi Soltani).

https://doi.org/10.1016/j.ccst.2024.100202
Received 9 November 2023; Received in revised form 13 January 2024; Accepted 4 February 2024

Nomenclature

ATR	autothermal reforming
BEIS	department for business, energy and industrial strategy
CCS	carbon capture & storage
CLC	chemical-looping combustion
CND	condenser
GHG	greenhouse gas emissions
HX	heat exchangers
KPIs	key performance indicators
LCOH	levelised cost of hydrogen
MEA	monoethanolamine
PCC	post-combustion carbon capture
PSA	pressure swing adsorption
SE-CL-SMR	sorption-enhanced chemical-looping steam methane reforming
SE-SMR	sorption-enhanced steam methane reforming
SE-SMR-CLC	sorption-enhanced steam methane reforming with chemical-looping combustion
SE-SMR-PCC	sorption-enhanced steam methane reforming with post-combustion carbon capture
SMR	steam methane reforming
TRL	technology readiness level
WGS	water gas shift

black (Chew et al., 2023). The hydrogen economy must incorporate low-carbon hydrogen production to ensure the mitigation and reduction of the effects of climate change (Ishaq et al., 2022), and at the same time, facilitate a smooth transition into net zero. As of 2021, 94 million tonnes (Mt) of hydrogen were produced globally; the breakdown of how the hydrogen is produced is shown in Fig. 1 (IEA, 2022).

Currently, hydrogen production produces over 900 Mt of CO_2 a year globally (IEA, 2022). The majority of this is produced *via* the Steam Methane Reforming (SMR) or Autothermal Reforming (ATR) processes. Within the SMR process, the feedstock (i.e. methane and steam) are heated, pressurised and then introduced into a reformer (i.e. a reactor) where reactions (R1) and (R3) take place. The products are then transferred into a Water Gas Shift (WGS) reactor where reaction (R2)

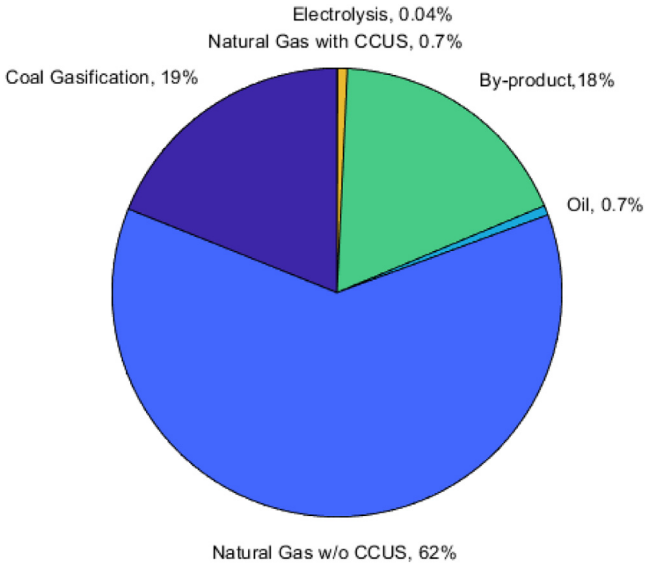

Fig. 1. Global hydrogen production routes as of 2021, data taken from (IEA, 2022).

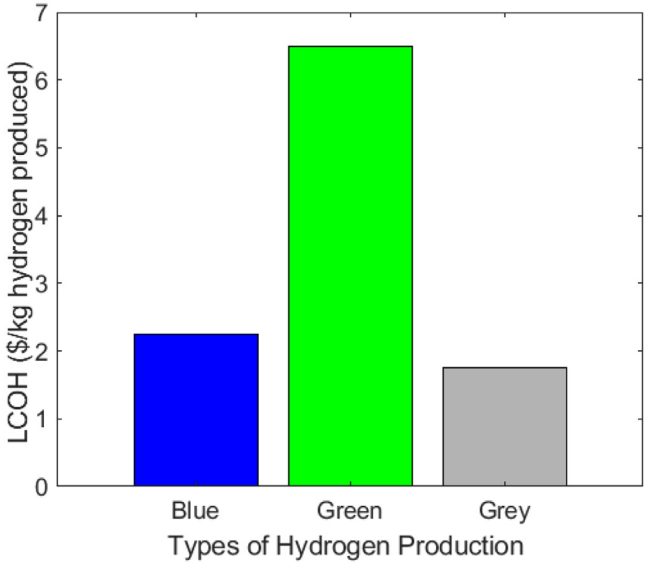

Fig. 2. Average LCOH of different hydrogen production methods in 2021 (IEA, 2022).

takes place. The H_2 and CO_2 gases are then transferred into a Pressure Swing Adsorption (PSA) unit where the produced H_2 is further purified to meet specific product specifications.

$$CH_{4(g)} + H_2O_{(g)} \leftrightarrow CO_{(g)} + 3H_{2(g)} \quad \Delta H_{298K} = 206.2 \text{ kJ mol}^{-1} \tag{R1}$$

$$CO_{(g)} + H_2O_{(g)} \leftrightarrow CO_{2(g)} + H_{2(g)} \quad \Delta H_{298K} = -41.2 \text{ kJ mol}^{-1} \tag{R2}$$

$$CH_{4(g)} + 2H_2O_{(g)} \leftrightarrow CO_{2(g)} + 4H_{2(g)} \quad \Delta H_{298K} = 165.2 \text{ kJ mol}^{-1} \tag{R3}$$

Global blue and green hydrogen production rates are currently extremely low, accounting for 0.74 Mt and 0.042 Mt, respectively (IEA, 2022), as grey hydrogen dominates (blue hydrogen but without the CCS). However, this is projected to change by 2030 as blue and green hydrogen production is expected to increase to 10 Mt and 14 Mt respectively (IEA, 2022). Within the UK, there has been a recent policy by the Department for Business, Energy and Industry (BEIS) in which new hydrogen production projects must capture 95 % of CO_2 produced (EA, 2023). Low-carbon hydrogen production has a key role in reducing GHG emissions. Currently, green hydrogen production is a much more expensive option with a higher levelised cost of hydrogen (LCOH), while blue hydrogen production has a lower LCOH, as shown in Fig. 2. This signifies the importance of timely scale-up of blue hydrogen production.

Sorption-Enhanced Steam Methane Reforming (SE-SMR) is a relatively new process configuration with potential to replace the more conventional (SMR/ATR + carbon capture) processes. SE-SMR incorporates a high-temperature sorbent like CaO in the SMR reformer, the sorbent then captures CO_2 in-situ within the reformer as described by reaction (R4). The $CaCO_3$ is then transferred into the calciner *via* an interconnected fluidised bed system (HyPER, 2019). This process intensification aims to develop a process that is significantly more economical in comparison to conventional blue hydrogen production. Furthermore, introducing CaO into the reformer helps to increase H_2 purity together with increased CH_4 conversion rates due to the Le Chateliers principle (Tzanetis et al., 2012). As described by reaction (R4), the carbonation of CaO is exothermic and therefore, the liberated energy can drive the endothermic reforming reaction. The lowering of the reforming temperature also provides a reduction in the sintering and coking of catalysts - a key issue within the SMR processes (Masoudi Soltani et al., 2021).

$$CaO_{(s)} + CO_{2(g)} \leftrightarrow CaCO_{3(s)} \quad \Delta H_{298K} = -178.8 \text{ kJ mol}^{-1} \tag{R4}$$

Currently, SE-SMR is at technology readiness level (TRL) five. Recent work has focused on elevating this TRL through the HyPER project (HyPER, 2019) . Furthermore, to facilitate a more confident scale-up approach, process modelling is required to identify optimum operating conditions that aim to enhance the key performance indicators (KPIs) of the process. Analysis of these process models is important to ensure that an optimum process configuration and process performance is achieved (Davies et al., 2023). One such method is exergy analysis which is defined as the maximum amount of useful work available within a system as it is bought into equilibrium with reference environment (Simpson and Lutz, 2007). Exergy analysis combines both the second law of thermodynamics with the conservation of mass and heat transfer to provide a realistic insight into the true thermodynamic efficiency of a process (Tzanetis et al., 2012). It can significantly facilitate the identification of inefficiencies within the process and can identify where thermodynamic losses occur within the process in comparison to conventional energy analysis which is based on the first law of thermodynamics.

1.2. Literature review

As mentioned above, there has been a vast array of literature on the process modelling and subsequent thermodynamic analysis of blue hydrogen production process. (Yan et al., 2020b) assessed the performance of six different process configurations of SE-SMR using five KPIs (CH_4 conversion, H_2 purity, cold gas efficiency, net efficiency, CO_2 capture efficiency) and found that incorporating Chemical-looping Combustion (CLC) (iron oxide chosen as the O_2 carrier) into the process provided the best performance with respect to the pre-defined KPIs. Antzara et al. (2015) performed a thermodynamic analysis on a novel Sorption-enhanced Chemical Looping Steam Methane Reforming (SE-CL-SMR) process and assessed the thermodynamic performance in comparison with both SE-SMR and SMR process and found that the SE-CL-SMR process reduces the energy requirements up to 55 % in comparison to SMR.

Although an energy analysis is useful to gauge an idea of the thermodynamic efficiency of the whole process, as mentioned earlier, exergy analysis provides a more in-depth analysis of the process. Exergy analysis has been applied to the SMR process. Simpson and Lutz (2007) carried out an exergy analysis of SMR and assessed the impact of key operating parameters of the reformer and their impact on exergy efficiency. In another study, Hajjaji et al. (2012) analysed the exergy of the SMR process and found that by implementing a heat recovery system, they were able to increase both the thermal and exergy efficiency by about 4 %. This showcases the effective use of exergy analysis as a tool for process improvement. Tzanetis et al. (2012) focused on a comparison between SMR and SE-SMR. It was realised that SE-SMR performed significantly better than SMR in terms of exergy analysis, both with and without a carbon capture unit. This highlights the fact that the incorporation of in-situ CO_2 capture provides improved thermal and exergy efficiency in comparison to retrofitting CCS. In their work, however, the incorporation of process improvements was overlooked.

1.3. Paper motivation

There is a considerable amount of scientific work assessing the performance of blue hydrogen production and the integration of CCS technologies into hydrogen production. These works, however, have mostly focused on thermal and energy efficiency. As of today, there is little research done on the exergy analysis of blue hydrogen production, specifically SE-SMR. To the best of the authors' knowledge, there has been no reported exergy analysis on SE-SMR with post-combustion carbon capture (PCC) looking into process improvement.

Based on the above discussion, this paper aims to advance the literature by identifying an optimum process configuration for the SE-SMR process *via* exergy analysis. By assessing the process through an exegetic lens, inefficiencies are better pinpointed within the process and can, therefore, improve the process design. The next section outlines the methodology of the study, in which the process modelling together with the exergy analysis methodology have been detailed. This is then followed by a comprehensive discussion of the results which then delves into the identification of process improvements within the system, why these inefficiencies occur and the subsequent process improvements of the said inefficiencies. The paper concludes with a discussion of future research opportunities in this area.

2. Methodology

2.1. Conceptual process design

A steady-state thermodynamic-based model was developed in Aspen Plus (version 12.1), based on previous work done by (Yan et al., 2020b). From this previous work case two was selected, shown in Fig. 3, as the conventional/baseline case due to its competitive performance with CLC whilst using a conventional combustion system. The baseline case provides a viable process for low-carbon hydrogen production with a further techno-economic analysis. It has shown that this process is a theoretically viable commercial process that can capture CO_2 and produce H_2 in a cost-effective manner (Yan et al., 2020a). This system can have an amine scrubbing system retrofitted to the combustion system to develop a low-carbon hydrogen production process in line with the current commercial approach to PCC.

The process was adapted to remove the heat exchanger (HX) network to develop a baseline case. A PCC unit (i.e. an amine scrubber with 30 wt.% monoethanolamine (MEA)) was added to the process. Fig. 4 demonstrates the simplified process flowsheet of this SE-SMR process. The process involves CH_4 and H_2O being heated and pressurised. These streams enter the reformer (with CaO entering the reformer *via* the calciner), where (R1)–(R4) occur. The H_2 that forms, leave the reformer and is then purified *via* a knockout drum and a PSA unit. The $CaCO_3$ produced in the reformer, enters the calciner in which the reverse of (R4) occurs. The heat required for the calciner is provided by the combustion unit, which uses CH_4 as the reactant. The flue gas produced is then transferred into the PCC system where MEA absorbs the CO_2. This CO_2-rich MEA is then transferred to the desorber where the CO_2 is stripped off.

Table 1 highlights the operating conditions and design assumptions for each equipment/unit operation. Peng–Robinson was used as the thermodynamic package for the SE-SMR process, with (R1)–(R4) taking place in the reformer and calciner. The operating conditions were

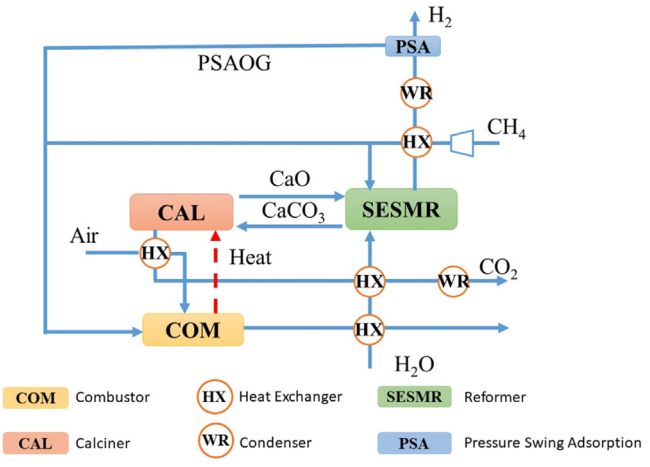

Fig. 3. Simplified SE-SMR + PSA process flowsheet of process (Case 2), adapted from (Yan et al., 2020b).

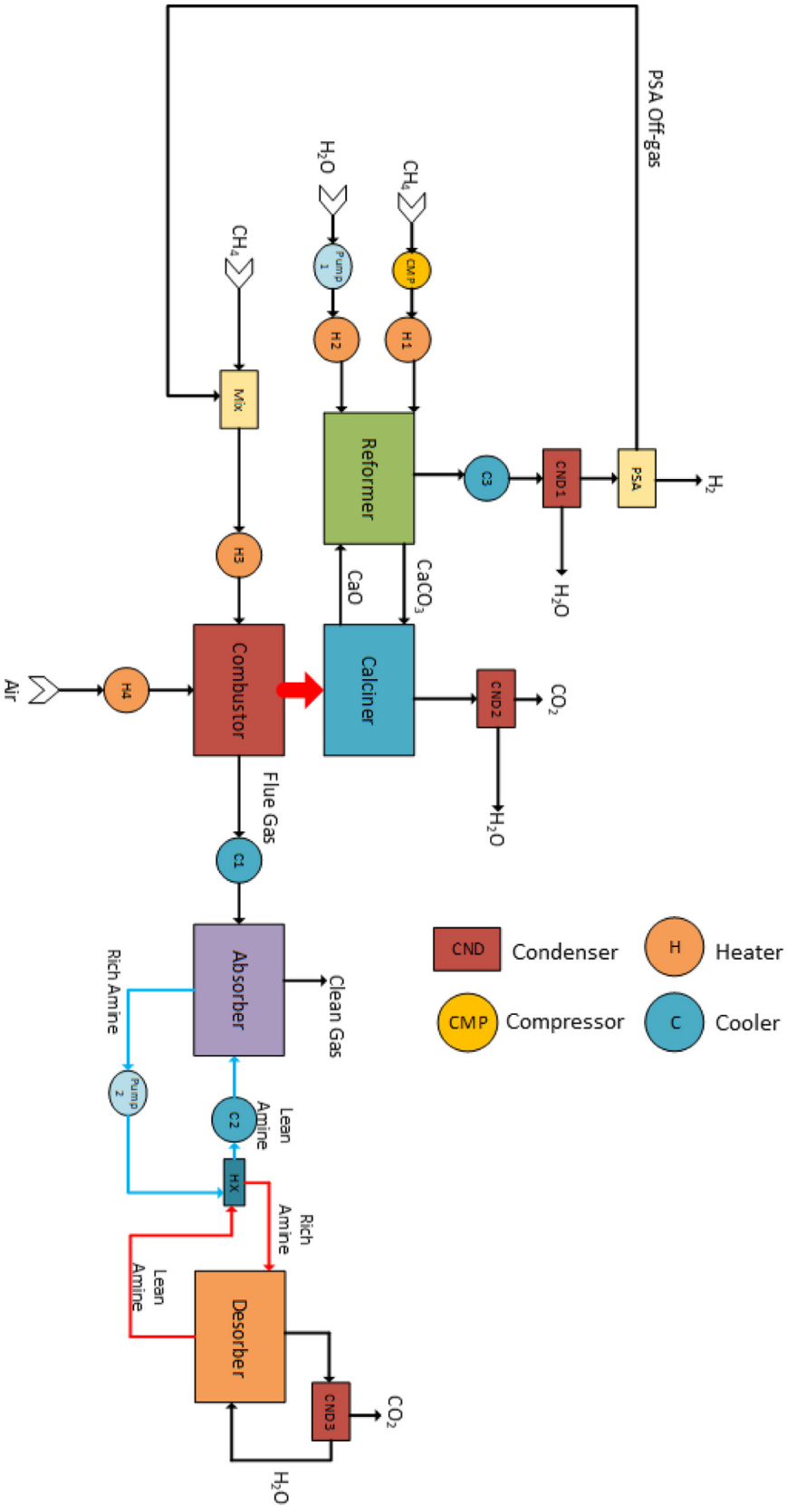

Fig. 4. Simplified process flowsheet of SE-SMR process with PCC.

Table 1
Operating conditions of unit operators within the process.

Stream/Block	Components	Temperature (°C)	Pressure (bara)
CH_4 in	100 % CH_4 Flow rate: 228 kmol/h	25	1
H_2O in	100 % H_2O Flow rate: 1138 kmol/h	25	1
Amine in	MEA (30% wt) H_2O (70% wt) CO_2 Loading (0.21)	40	1.1
Compressor	Isentropic (83 %) Mechanical (98 %)	338	25
Pump	Pump (83 %)	25	25
Heater One (H1)	Heater	540	25
Heater Two (H2)	Heater	545	25
Heater Three (H3)	Heater	600	1
Heater Four (H4)	Heater	250	1
Cooler One (C1)	Heater	40	1
Cooler Two (C2)	Heater	40	2
Cooler Three (C3)	Heater	250	25
Cooler Four (C4)	Heater	250	Inlet: 1 Outlet: 1
Condenser One (CND1)	Flash2	25	25
Condenser Two (CND2)	Flash2	25	1
Condenser Three (CND3)	Flash2	20	2
PSA	Separator	25	25
Reformer	RGibbs	640	25
Calciner	RGibbs	900	1
Desorber	Radfrac	90–124	2
Absorber	Radfrac	40–58	1
Heat Exchanger	MHeatX	Hot stream: 124–94 Cold stream: 58–90	2
Combustor	RGibbs	1000	1

based off of (Yan et al., 2020b) in which the optimal operating conditions were found. The reformer and calciner were modelled using the RGibbs reactor which aims to minimise the Gibbs free energy of all the chemical species within the system. The PSA unit is designed so that the PSA off-gas is recycled into the combustion system.

For the amine scrubber, E-NRTL was used as the thermodynamic package. MEA was chosen as the solvent for the PCC unit. Reactions (R5)–(R9) describe the reactions that take place between CO_2 and MEA. For the PCC system, radfrac columns were selected as the absorber and stripping columns.

$$2H_2O \leftrightarrow H_3O^+ + OH^- \tag{R5}$$

$$CO_2 + H_2O \leftrightarrow H_3O^+ + HCO_3^- \tag{R6}$$

$$HCO_3^- + H_2O \leftrightarrow H_3O^+ + CO_3^{2-} \tag{R7}$$

$$H_2O + MEACOO^- \leftrightarrow MEA + HCO_3^- \tag{R8}$$

$$MEA + H_3O^+ \leftrightarrow H_2O + MEA^+ \tag{R9}$$

The model assumptions include: steady-state operation, zero pressure drop, no temperature gradient within the reactor and no pressure drop within the process. These were selected to reduce the model complexity without significantly affecting the results which have been validated with experimental data.

2.2. Exergy analysis

Exergy analysis was done *via* Microsoft Excel and Aspen Plus (version 12.1). In order to calculate the exergy of individual streams, Eq. (1) is used.

$$E_{stream} = E_{ph} + E_{ch} + E_{ke} + E_{pe} \tag{1}$$

where E_{stream} is the exergy of a stream within the system, E_{ph} is the physical exergy, E_{ch} is the chemical exergy, E_{ke} is the kinetic exergy, and E_{pe} is the potential exergy. In this work, the kinetic exergy and potential exergy are assumed to be negligible. To calculate the physical exergy Eq. (2) is used.

$$E_{ph} = (h - h_0) - T_0(s - s_0) \tag{2}$$

h and h_0 are the enthalpy of the system and the enthalpy of the system at the reference environment, respectively. T_0 is the temperature of the reference environment, s and s_0 are the entropy of the system and the entropy of the system at the reference environment, respectively. The reference temperature and pressure are 298.15 K and 1 atm, respectively. To calculate the chemical exergy, Eq. (3) is used.

$$E_{ch} = \sum_i x_i E_{ch,i} + RT_0 \sum_i x_i ln(x_i) \tag{3}$$

x_i is the mole fraction, $E_{ch,i}$the standard chemical exergy of compound i (kJ mol^{-1}) and R is the universal gas constant. In order to calculate the chemical exergy for non-ideal liquid streams, Eq. (4) is used.

$$E_{ch} = \sum_i x_i E_{ch,i} + RT_0 \sum_i x_i ln(\gamma_i x_i) \tag{4}$$

where γ_i is the fugacity of the stream. The chemical exergy of an individual component has either been taken from literature or calculated *via* Eq. (5).

$$0 = \sum_i v_i (E_{ch,i} - g_{f,i}) \tag{5}$$

where v_i is the stoichiometric coefficient, and $g_{f,i}$is the standard Gibbs free energy of formation of compound i (kJ mol^{-1}). This can be rearranged to calculate the exergy of individual components of the reaction as shown through Eqs. (6)–(9).

$$0 = v_j (E_{ch,j} - g_{f,i}) + \sum_i v_i (E_{ch,i} - g_{f,i}) \tag{6}$$

$$-\sum_i v_i (E_{ch,i} - g_{f,i}) = v_j (E_{ch,j} - g_{f,i}) \tag{7}$$

Table 2
Chemical exergy values of individual components.

Name of compound	Chemical exergy value (kJ/mol)	References
N_2	0.72	(Szargut, 1989)
O_2	3.97	(Szargut, 1989)
CO	274.71	(Szargut, 1989)
CO_2	19.48	(Szargut, 1989)
$CaCO_3$	16.30	(Szargut, 1989)
CaO	127.3	(Szargut, 1989)
H_2	236.09	(Szargut, 1989)
H_2O (g)	9.5 0	(Szargut, 1989)
CH_4	831.20	(Szargut, 1989)
Fe_2O_3	12.40	(Szargut, 1989)
Al_2O_3	15.00	(Szargut, 1989)
SiO_2	2.2	(Szargut, 1989)
Fe	374.3	(Szargut, 1989)
Fe_3O_4	116.30	(Szargut, 1989)
Ni	232.70	(Szargut, 1989)
NiO	23.00	(Szargut, 1989)
MEA	1544.88	(Mohamadi-Baghmolaei et al., 2021)
$MEAH^+$	1246.95	Calculated
$MEACOO^-$	1818.47	Calculated
CO_3^{2-}	−23.10	Calculated
HCO_3^-	16.89	(Mohamadi-Baghmolaei et al., 2021)
OH^-	1.23	Calculated
H_3O^+	942.79	Calculated
H_2O (l)	0.90	(Szargut, 1989)

$$-\frac{1}{v_j}\sum_i v_i\left(E_{ch,i}-g_{f,i}\right)=E_{ch,j}-g_{f,i} \tag{8}$$

$$E_{ch,j}=g_{f,j}-\frac{1}{v_j}\sum_i v_i\left(E_{ch,i}-g_{f,i}\right) \tag{9}$$

With $E_{ch,j}$ being the chemical exergy of the unknown component. The calculated individual chemical exergy values are shown in Table 2. The values were either taken from the literature or calculated.

To calculate the exergy in a stream with respect to heat transfer, Eq. (10) is used.

$$E_q=q\times\left(1-\frac{T_0}{T}\right) \tag{10}$$

E_q is the exergy *via* heat transfer, q is the heat duty, T_0 is the temperature at the reference environment and T is the stream temperature. In order to calculate the exergy destruction and exergy efficiency of the whole process (i.e. two of the KPIs studied in this work), Eqs. (11) and (12) are employed.

$$Exergy\ Destroyed=\sum Exergy\ In-\sum Exergy\ Out \tag{11}$$

$$Exergy\ Efficiency=\frac{Exergy\ Out\ H_2\ Stream}{Total\ Exergy\ In}\times 100 \tag{12}$$

The other three KPIs in this work (i.e. CO_2 capture rate, H_2 purity, thermal efficiency) have been defined *via* Eqs. (13)–(15), respectively.

$$CO_2\ Capture\ Rate=\frac{n_{CH_4\ in}-n_{CH_4\ out}-n_{CO\ out}-n_{CO_2\ out}}{n_{CH_4\ in}}\times 100 \tag{13}$$

$$H_2\ Purity=\frac{n_{H_2out}}{n_{H_2\ out}+n_{CH_4\ out}+n_{CO\ out}+n_{CO_2\ out}}\times 100 \tag{14}$$

$$Thermal\ Efficency=\frac{n_{H_2out}\times LHV\,H_2}{n_{CH_4\ in}\times LHVCH_4+W_{com}+W_{pumps}+Q_{reboiler}} \tag{15}$$

For the exergy destruction and exergy efficiency within individual components, Eqs. (12) and (16) have been used. Eq. (16) can also be used to calculate the exergy efficiency of the whole process as well.

$$Ex_{ic}=\frac{1-Exergy\ Destroyed}{Exergy\ In}\times 100 \tag{16}$$

where Ex_{ic} is the exergy efficiency of individual components. In order to account for exergy destruction within the pump and compressor, Eq. (17) is used.

$$Ex_{p/c}=\sum Exergy\ In-\sum Exergy\ Out+W_{c/p} \tag{17}$$

where $Ex_{p/c}$ is the exergy destruction of the pump or compressor, and $W_{c/p}$ is the work of the compressor or pump. In order to account for the exergy destruction of heaters or coolers, Eq. (18) is used.

$$Ex_{h/c}=\sum Exergy\ In-\sum Exergy\ Out+E_q \tag{18}$$

where $Ex_{h/c}$ is the exergy destruction within a heater or cooler, and E_q is the exergy of the heat transfer. In order to calculate the exergy destruction of the combustion chamber, Eq. (19) is used.

$$Ex_{comb}=\sum Exergy\ In-\sum Exergy\ Out+E_{fuel} \tag{19}$$

where Ex_{comb} is the exergy destruction in the combustor, and E_{fuel} is the chemical exergy of the fuel.

3. Results & discussion

3.1. Validation of the baseline system

3.1.1. Validation of SE-SMR system

To validate the SE-SMR model, the concentrations of gases leaving the reformer were calculated and compared with experimental data reported in the literature (García et al., 2020; Johnsen et al., 2006). The model was run under the following conditions: reformer temperature = 600 °C, S/C ratio = 6, reformer pressure = 1 atm. The results are shown in Table 3.

As shown in Table 3 the SE-SMR process shows excellent agreement with previous experimental work.

3.1.2. Validation of amine scrubbing system

To validate the PCC process, experimental data from Kwak et al. (2012) was used. The regeneration energy for a 90 % CO_2 capture rate was compared at different L/G ratios for each process, with Fig. 5 below showcasing the results.

As shown in Fig. 5, there is a good agreement between the experimental data and the data the model has produced.

3.2. Exergy analysis of SE-SMR: a new comparative baseline

The exergy analysis of the SE-SMR process shows that across the whole process, most of the exergy entering the system comes from the methane inlet which is then subsequently reformed as shown in Table 4 and Fig. 6. The main contribution of exergy leaving the system is a result of the H_2 being produced and exergy being destroyed, as

Table 3
comparison of gas concentration leaving the reformer.

	H_2 (% dry)	CH_4 (% dry)	CO (% dry)	CO_2 (% dry)
This study	98.3	0.146	0.31	0.853
(García et al., 2020)	98.4	~0.2	~0.2	~1
(Johnsen et al., 2006)	98	1	0.5	0.5

Table 4
Exergy entering and leaving the system.

Exergy analysis of the whole system			
Exergy streams entering the system	Exergy in values (kW)	Exergy streams leaving the system	Exergy out values (kW)
Methane (reforming)	52,550.19	Hydrogen (Product)	50,447.15
Water (reforming)	284.51	Carbon Dioxide (Calciner)	1052.09
Methane (fuel)	13,107.80	Water (Condenser)	1967.79
Heat Duty	5771.13	Carbon Dioxide (Desorber)	457.69
Compressor	886.50	Clean Gas (Absorber)	15.75
Pump One	17.47	Exergy Destruction	24,001.88
Air	32.41		
Reboiler Duty	5200.00		
Pump Two	2.59		
Recycled Water	11.71		
Recycled MEA	78.02		

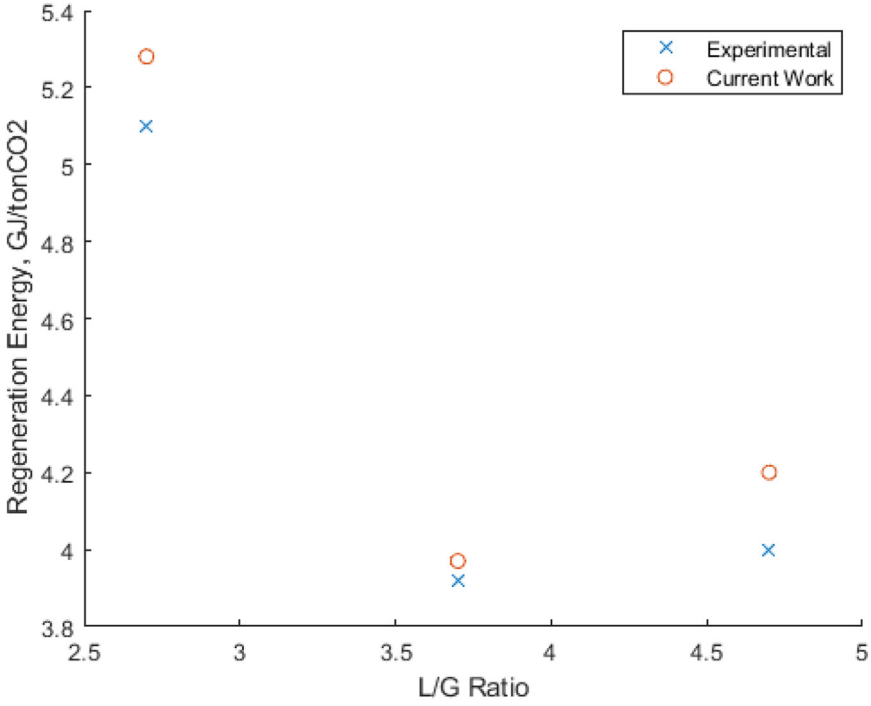

Fig. 5. Validation of the PCC system by comparing the change in regeneration energies at different L/G ratios.

Table 5
KPI comparison with previous literature.

Reference	Process	H_2 purity (%)	CO_2 capture rate (%)	Thermal efficiency (%)	Exergy efficiency *via* Eq. (12) (%)	Exergy efficiency *via* Eq. (16) (%)
This paper	SE-SMR	99.99	96.04	71.97	64.67	69.21
(Simpson and Lutz, 2007)	SMR	N/A	0	66.70	62.69	N/A
(Hajjaji et al., 2012)	SMR	N/A	0	70	N/A	73.32
(Hajjaji et al., 2012)	SMR	N/A	0	73.9	N/A	74.77
(Tzanetis et al., 2012)	SE-SMR	89.4	N/A	N/A	N/A	78.07
(Tzanetis et al., 2012)	SMR	89.4	0	N/A	N/A	75.6

shown in Fig. 6. A comparative assessment of the five KPIs of this process with the literature data has been made and summarised in Table 5.

The table highlights the comparable exergy and thermal efficiency of this process in comparison to SMR. The in-situ CO_2 capture *via* calcium looping allows for an improved process efficiency, making it competitive even with conventional SMR without any additional carbon capture units retrofitted to the process. Some processes have a greater efficiency with respect to exergy, although they overlook the inclusion of CO_2 capture technology on the combustion unit. Although this process has a high thermal and exegetic efficiency with an improved CO_2 capture rate, exergy destruction still occurs. Table 6 showcases the exergy destruction and efficiency of individual components within the process, with Fig. 7 providing an illustrative comparison of the exergy destruction taking place within the process.

Most of the exergy destruction occurs in the heating and cooling, combustion, and PCC systems as summarised in Table 6. There is contribution *via* the reforming process as well. Within the reforming process, the overall reaction is described *via* (R10).

$$CH_{4(g)} + 2H_2O_{(g)} + CaO_{(s)} \leftrightarrow CaCO_{3(s)} + 4H_{2(g)} \quad \Delta H_{298K} = -13.6 \text{ kJ mol}^{-1} \tag{R10}$$

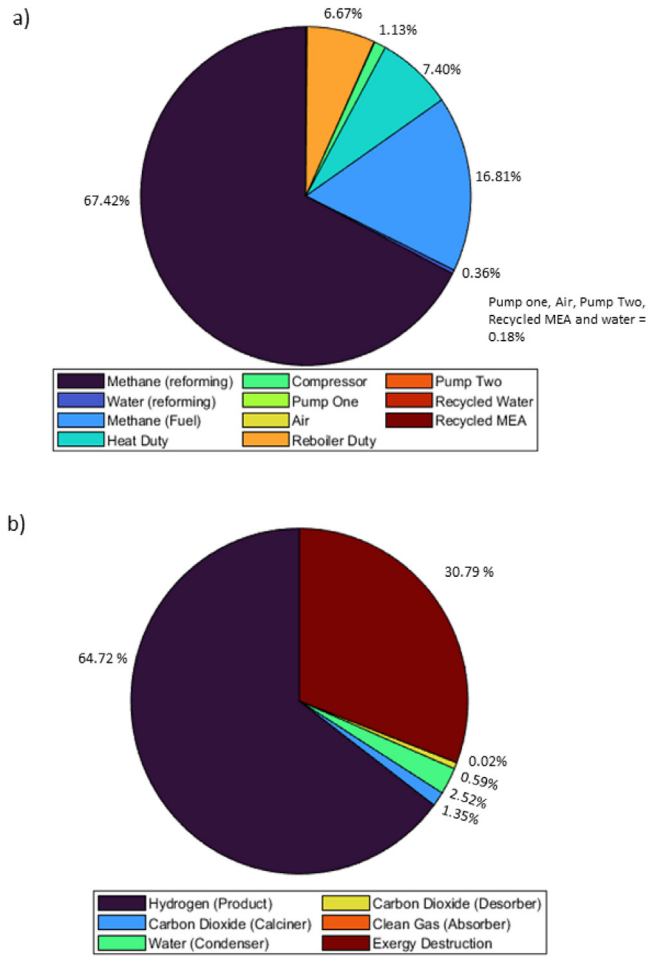

Fig. 6. Breakdown of exergy entering the system (a) and leaving the system (b).

The exothermic nature of the reaction occurring within the reformer accounts for the exergy destruction as heat is being released into the environment. As well there is an increased entropy within the system as more gaseous products are produced, accounting for some of the exergy destruction also. Although the exergy destruction is high, it is an exegetically efficient unit with an exergy efficiency of 98.5 %. This increase in efficiency is due to the incorporation of the solid sorbent, the overall temperature of the sorption-enhanced reactor is reduced in comparison to a conventional reforming reactor.

The main contribution to the exergy destruction within the process is the heating and cooling of the reactants and products, the contribution of this system to the overall exergy destruction is 40.29 %. This high exergy destruction value is a result of the phase change of the H_2O from a gaseous to a liquid state and vice versa at increased pressure; the chemical exergy of the gaseous and liquid H_2O is 9.5 and 0.9 kJ/mol, respectively. This noticeable difference in chemical exergy accounts for the exergy destruction observed. Although these phase changes at high pressures account for exergy destruction, the high pressure drives the reaction to favour hydrogen production (i.e. increased product yield).

Table 6
Exergy destruction and efficiency of individual components.

Individual component	Exergy destruction (kW)	Exergy efficiency (%)	Contribution to total exergy destruction (%)
Combustor	5961.62	57.52	24.84
C1	3472.68	30.83	14.47
C3	2632.87	96.04	10.97
Desorber	1935.25	98.35	8.06
H2	1788.17	86.66	7.45
Mixer	1575.56	98.07	6.56
CND1	1523.46	97.62	6.35
Absorber	1315.65	98.93	5.48
Reformer	1174.24	98.54	4.89
HX	760.86	99.66	3.17
CND3	462.18	52.95	1.93
Air Heater	392.02	60.81	1.63
C2	286.48	99.73	1.19
Fuel Heater	174.57	99.26	0.73
C4	133.45	96.11	0.56
CND2	133.33	88.75	0.56
PSA	101.25	99.83	0.42
Compressor	92.47	99.83	0.39
H1	39.83	99.93	0.17
Mixer	21.34	99.91	0.09
Calciner	11.55	99.94	0.05
Mixer	9.70	99.99	0.04
Pump 1	1.72	99.43	0.01
Pump 2	1.62	100.00	0.01
Separator	0.00	100.00	0.00

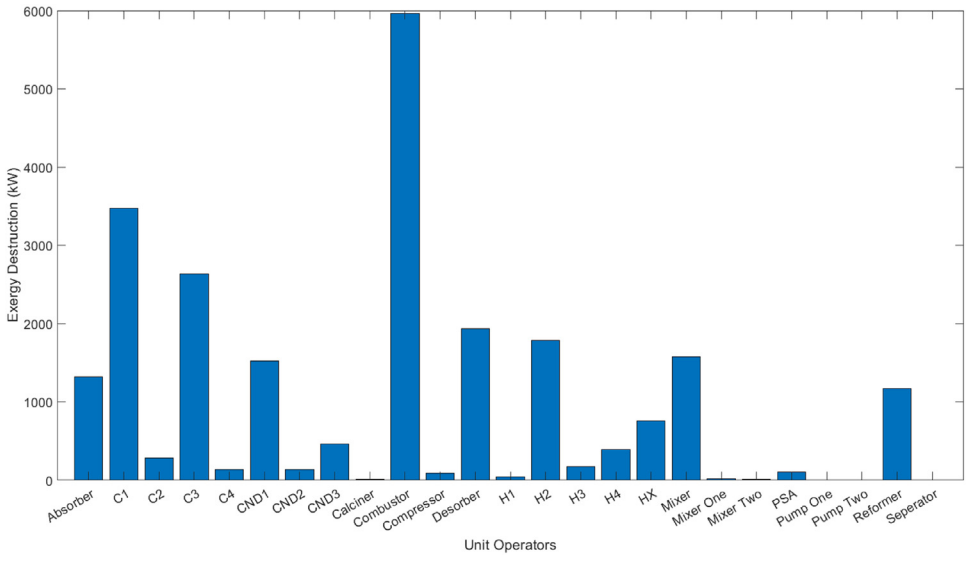

Fig. 7. Comparison of exergy destruction within the process.

Within the combustion system, there is a high level of exergy destruction (5961.62 kW). This unit is not particularly exergy efficient (57.51 %) either. It is in fact, the unit with the greatest contribution to the exergy destruction (24.83 %) in the process. This is due to the irreversible nature of the combustion reaction of methane as shown in (R11) as well as the incomplete combustion. The process is almost an irreversible process; this is realised by considering how exothermic the process is and the difference in the chemical exergy of the reactants (CH_4 = 831.2 kJ/mol) and the products (CO_2 = 19.2 kJ/mol).

$$CH_{4(g)} + 2O_{2(g)} \leftrightarrow CO_{2(g)} + 2H_2O_{(g)}\ \Delta H_{298K} = -891\ \text{kJ mol}^{-1} \quad \text{(R11)}$$

When using an amine scrubber, the cooling of the flue gas before entering the absorber is extremely exegetically inefficient with an exergy efficiency of only 7 %. Amine scrubbers are, however, essential to meeting a 95 % CO_2 capture rate. These additional processes result in a decrease in the exergy efficiency of the overall process, with the majority of such inefficiencies linked to the absorber and desorber. Within the absorber, exergy destruction is associated with temperature change within the reformer as a result of the exothermic nature of the absorption of CO_2 in the MEA solution. The exothermic nature of the absorption of CO_2 and the formation of ions explain the exergy destruction in the absorber. The impact of CO_2 loading is a key factor in the efficiency of the process. As reported by Soltani et al. (2017), a CO_2 loading of 0.21 allows for a reduced energy required for the amount of CO_2 captured.

There is a higher exergy destruction occurring in the desorber due to the increased heat requirement for the process of stripping the CO_2 from the MEA. The increased heat and slight increase in pressure are advantageous for this process. The heat is generated by the reboiler which is effectively used for three purposes:

1. Latent heat of vaporisation of water;
2. Heat required for the stripping of the CO_2 from the MEA;
3. Temperature change across the desorber.

The temperature change within the desorber and the phase change of the water accounts for the exergy destruction within the desorber. In the sorption-enhanced steam methane reforming with post-combustion carbon capture (SE-SMR-PCC), there are three main areas in which the process can be improved. The heating and cooling system, the combustion system and the PCC system.

3.3. Retrofitting CLC to SE-SMR

3.3.1. Conceptual process synthesis and design

As highlighted in Section 3.1, most of the exergy destruction within the process occurs in the combustion system followed by the PCC unit. Utilising a conventional combustion system, a PCC system is required to ensure the CO_2 produced is captured and stored. However, this process is highly irreversible meaning a reduced exergy efficiency. As well, the extra steps to separate the CO_2, consume a large amount of energy. These reasons mean that it contributes to high exergy destruction and significantly lowers the efficiency of the process.

To improve the efficiency of the process, a CLC unit was added to the process, whilst removing the combustion and PCC to form the sorption-enhanced steam methane reforming process with chemical-looping combustion (SE-SMR-CLC). The process block diagram is shown in Fig. 8. Table 7 highlights the operating conditions in this process. An exergy analysis was performed on the process to assess the relative performance.

The CLC process uses iron oxide as the oxygen carrier. This is selected due to the lower cost of iron oxide in comparison to alternatives such as nickel or cobalt. In this process, reduced iron oxide (Fe_3O_4) is oxidized by interacting with air in the air reactor. The oxidized iron oxide (Fe_2O_3) is then sent to the fuel reactor in which the iron oxide is reduced using CH_4. Due to the use of the PSA off-gas (including CO and H_2), there are competing reactions in which H_2 and CO act as reducing agents. The

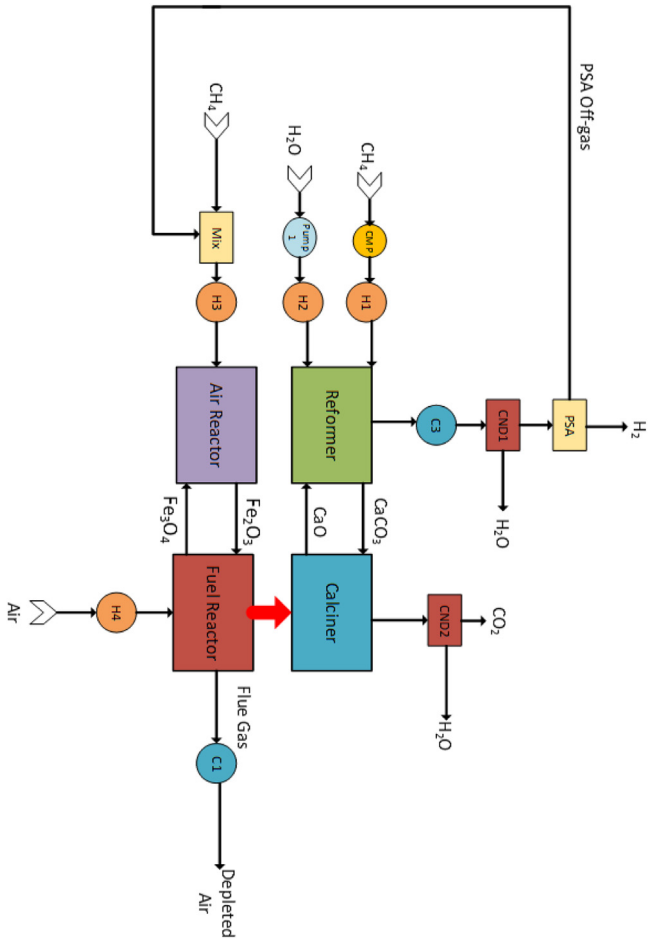

Fig. 8. SE-SMR-CLC simplified process flow diagram.

reaction scheme for the fuel reactor when CH_4, CO and H_2 are used as the reducing agents is described through reactions (R12)–(R14).

$$CH_4 + 12Fe_2O_3 \leftrightarrow 8Fe_3O_4 + CO_2 + 2H_2O\ \Delta H^{O}_{298} = 126.38\ \text{kJ mol}^{-1} \quad \text{(R12)}$$

$$H_2 + 3Fe_2O_3 \leftrightarrow 2Fe_3O_4 + H_2O\ \Delta H^{O}_{298} = 16.10\ \text{kJ mol}^{-1} \quad \text{(R13)}$$

$$CO + 3Fe_2O_3 \leftrightarrow 2Fe_3O_4 + CO_2\ \Delta H^{O}_{298} = -25.10\ \text{kJ mol}^{-1} \quad \text{(R14)}$$

R15 occurs in the air reactor when Fe_3O_4 and Fe_2O_3 are used as oxygen carriers.

$$4Fe_3O_4 + O_2 \leftrightarrow 6Fe_2O_3\ \Delta H^{o}_{298} = -534.54\ \text{kJ mol}^{-1} \quad \text{(R15)}$$

CLC is a method of combustion in which oxygen is introduced to the fuel *via* an oxygen carrier. This process is exegetically and thermally efficient compared to conventional combustion (Fan et al., 2016). The process has been shown to be more economical, although that is dependent on the choice of the oxygen carrier (Yan et al., 2020a). Another advantage of using a CLC system is that it separates the oxygen from the nitrogen in the air, meaning that when combustion occurs no NO_x emissions are produced theoretically, only CO_2 and H_2O are produced. This cleaner combustion alleviates the need for further separation of CO_2 from the flue gas.

3.3.2. Exergy analysis of SE-SMR with CLC

Exergy analysis of the system highlights the improved process efficiency by incorporating CLC into the process. Table 8 compares the SE-SMR-CLC with the SE-SMR-PCC process.

Table 7
Design assumptions for SE-SMR-CLC process.

Stream/Block	Composition	Temperature (°C)	Pressure (Bara)
CH_4 in	100 % CH_4 Flow rate: 224.724 kmol/h	25	1
H_2O in	100 % H_2O Flow rate: 1123.62 kmol/h	20	1
Compressor	Isentropic (83 %) Mechanical (98 %)	Inlet: 25 Outlet: 316	25
Pump	Pump (83 %) Driver (98 %)	20	25
Air Reactor	RGibbs	1300	1
Fuel Reactor	RGibbs	1341	1
Reformer	RGibbs	597	25
Calciner	RGibbs	900	1
Heater One	Heater	500	25
Heater Two	Heater	550	25
Heater Three	Heater	600	1
Heater Four	Heater	600	1
Cooler One	Heater	160	1
Cooler Two	Heater	170	25
Cooler Three	Heater	250	1
Condenser One	Flash 2	25	1
Condenser Two	Flash 2	25	1
PSA	Separator	25	25

Table 8
Comparison of KPIs of SE-SMR-CLC and SE-SMR-PCC system.

Process	H_2purity (%)	CO_2capture rate (%)	Thermal efficiency (%)	Exergy efficiency (%) *via* Eq. (12)	Exergy efficiency (%) *via* Eq. (16)	Exergy destroyed (kW)
SE-SMR-CLC	99.99	100	76.99	67.68	70.48	22,007.67
SE-SMR-PCC	99.99	96.04	71.97	64.67	69.21	24,001.86

Table 9
Exergy destruction and exergy efficiency of individual processing units in the SE-SMR-CLC process.

Processing unit	Exergy destruction (%)	Exergy efficiency (%)	Contribution to exergy destruction (kW)
Fuel Reactor	3931.58	98.10	17.86
C1	3694.83	7.53	16.78
C2	3176.18	95.07	14.43
H2	1880.04	85.95	8.54
Reformer	1796.89	97.72	8.16
Mixer	1557.81	98.06	7.07
CND1	1481.49	97.58	6.73
C3	1347.21	79.09	6.12
H4	1239.25	98.33	5.63
CND2	1076.46	98.55	4.89
Mixer	233.98	96.67	1.06
H3	173.63	99.28	0.78
Air Reactor	159.90	99.91	0.72
Compressor	107.43	99.79	0.48
PSA	56.36	99.91	0.25
Calciner	42.52	99.76	0.19
H1	35.04	99.93	0.15
Mixer	14.84	99.93	0.06
Pump 1	2.16	99.23	0.01

The above comparison of the processes underlines the improved performance of the process with respect to the KPIs when CLC is implemented. What is particularly noticeable is the higher CO_2 capture rate, whilst simultaneously boasting an increased thermal and exergy efficiency. This increased efficiency with respect to the thermal and exergy efficiency is the removal of the PCC unit, and more specifically, the reboiler which accounts for a high energy input into the system. The CLC is a more efficient combustion system as shown in Table 9 and Fig. 9. within the SE-SMR-CLC system, the sum of the exergy destruction in the air and fuel reactors sums to 4090 kW a reduction in comparison to the 5961 kW of exergy destruction occurring in the conventional combustion unit in the SE-SMR-PCC with a further about 4000 kW of exergy destruction in the PCC system. This improved exergy efficiency within the combustion unit is a result of an increase in the combustion efficiency of the process, due to the reversibility of the redox reaction that takes place in the combustion units. By utilising a reusable oxygen carrier, the process is reversible hence, an improvement in efficiency.

The fuel reactor is the processing unit with the highest contribution to the total exergy destruction within the system (17.86 %). This exergy destruction occurs as a result of the high temperature of the fuel reactor and the conversion of Fe_2O_3 to Fe_3O_4 which is not fully reduced. There is still some Fe_2O_3 leaving the fuel reactor and with the higher exergy

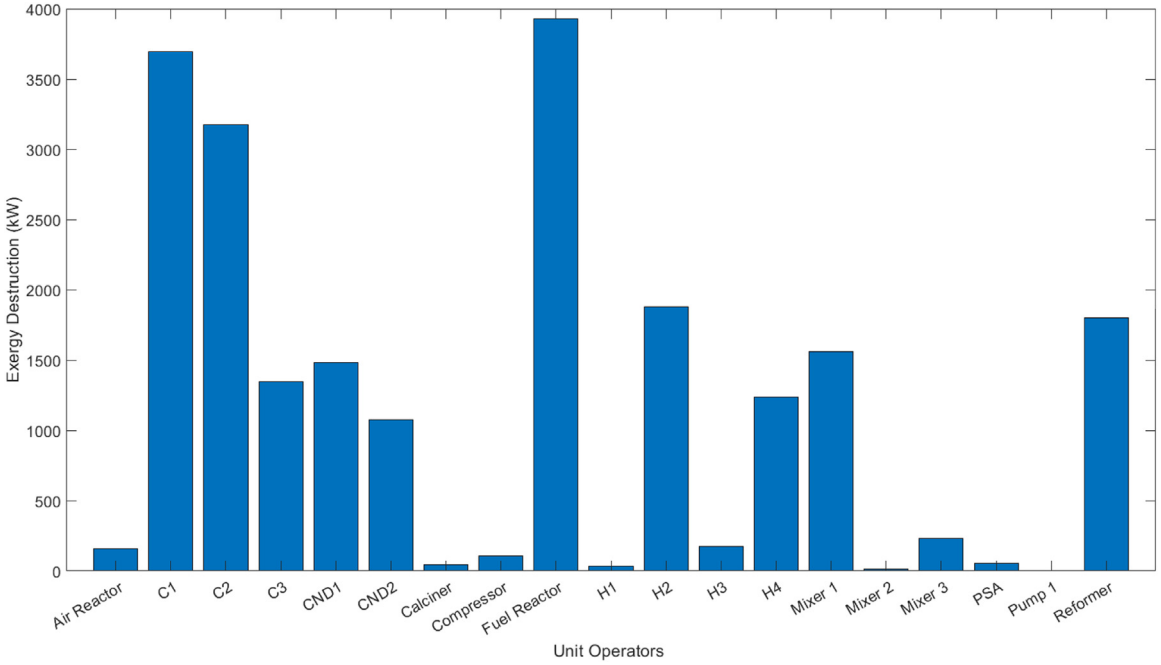

Fig. 9. Comparison of exergy destruction of individual processing units in SE-SMR-CLC process.

value of the reduced form of the iron oxide, a higher conversion rate is required to reduce the exergy destruction in the combustor. The use of H_2 as the reducing agent allows for a reduction of temperature in the fuel reactor, potentially reducing the exergy destruction in this process (Spreitzer and Schenk, 2019).

Although a further assessment of the design of the combustion system can be made, the majority of the exergy destruction is seen in the heating and cooling system (Table 9). As discussed previously, the current heating and cooling system accounts for a high exergy destruction and low exergy efficiency. Within the SE-SMR-CLC process the heating and cooling within the process accounts for over half of the total exergy destruction (52.43 %). Designing an efficient HX network is key to ensuring the waste heat can be repurposed in order to design a more energy and exergy-efficient process.

3.3.3. *Process heat intensification: heat integration* via *pinch analysis*

As mentioned, the heating and cooling system is an area in which a large exergy loss has been seen within both processes. In order to overcome this issue, a pinch analysis was implemented on the SE-SMR-CLC system to design an HX network that aims to recover energy within the system and consequently, improve the energy and exergy efficiency in the process. The HX developed was implemented on the system and then an exergy analysis was done to assess the process performance. An approach ΔT of 10 °C was selected in the analysis. The pinch point occurs at 21.3 °C with a minimum heat requirement of 1436.9 kW. A grand composite curve was developed as shown in Fig. 10. Based on this, a HX network was designed and implemented within the process and is shown in Fig. 11. Table 10 summarises the design assumptions.

The simulation was run, and an exergy analysis was performed with the results shown in Table 11.

A further assessment of the system shown in Table 12 and Fig. 12 highlights the exergy destruction within individual components. The development of the HX network reduces the total exergy destruction by a significant amount, and the repurposing of waste heat provides a significant increase in the exergy efficiency of the process. Table 12 and Fig. 12 show the exergy destruction and efficiency of individual components in the system as well as individual units' contribution to the exergy destruction.

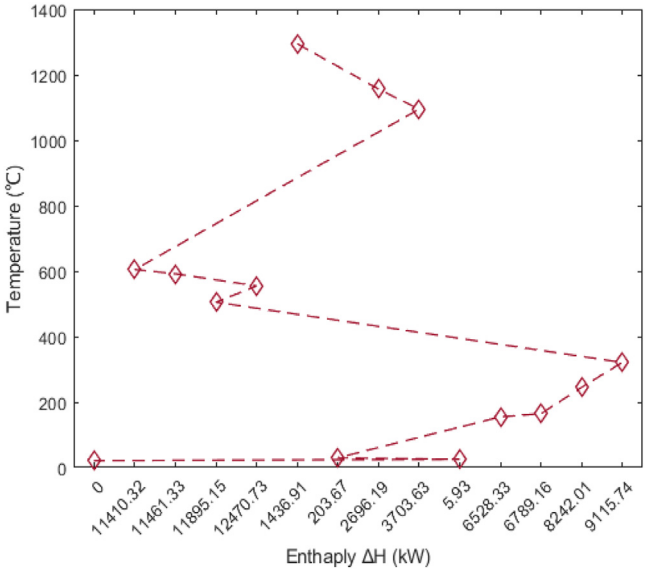

Fig. 10. Grand composite curve for SE-SMR-CLC process.

Assessment of the process shows a significant improvement in the heating and cooling system with a greater exergy efficiency and a reduction in exergy destruction. The greatest contribution to the exergy destruction is in the fuel reactor. The use of H_2 as the reducing agent could reduce the exergy destruction within the fuel reactor by increasing the efficiency of the combustion process.

3.3.4. *Impact of H_2 recycling on the efficiency of the CLC system*

The use of H_2 as a reducing agent in the CLC can improve the combustion efficiency to ensure a more efficient system. Hydrogen is recycled from the pure H_2 stream into the fuel reactor to be used as the reducing agent at prescribed percentages (i.e. 1 %, 5 %, 10 % molar). The result of this is shown in Table 13.

Recycling the H_2 produced as the reducing agent to the fuel reactor will slightly improve the exergy efficiency. This is due to the reduc-

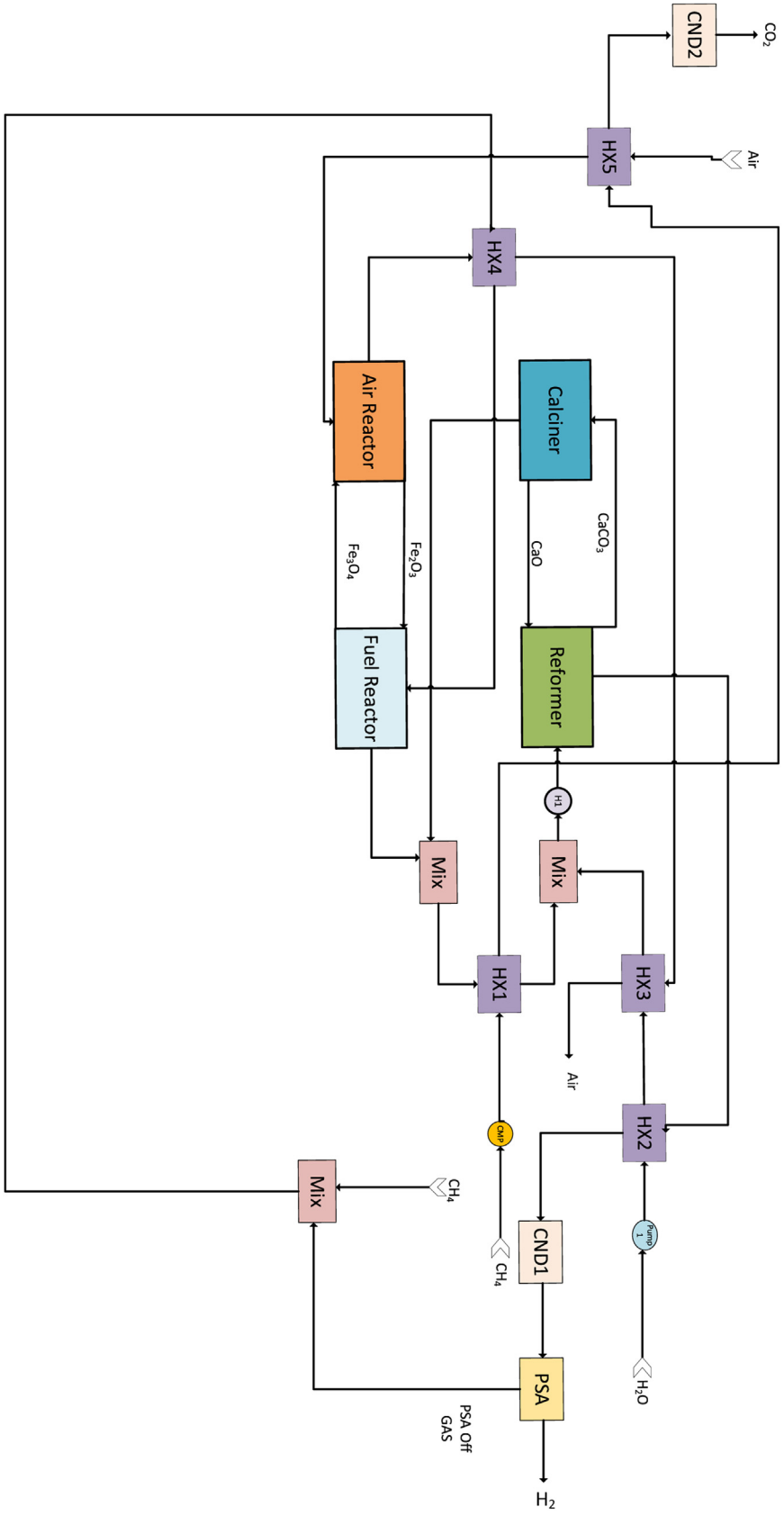

Fig. 11. Simplified process flow diagram of SE-SMR-CLC process with HX network.

Table 10
Design assumptions for SE-SMR-CLC system.

Stream/Block	Components	Temperature (°C)	Pressure (Bar)
CH_4 in	100 % CH_4	25	1
H_2O in	100 % H_2O	25	1
Reformer	RGibbs	600	25
Calciner	RGibbs	900	1
Air Reactor	RGibbs	1000	1
Fuel Reactor	RGibbs	1100	1
Heat Exchanger One	MHeatX	Cold stream inlet: 316 Cold stream outlet: 600 Hot stream inlet: 1100 Hot stream outlet: 842	Cold stream pressure: 25 Hot stream pressure: 1
Heat Exchanger Two	MHeatX	Cold stream inlet: 20 Cold stream outlet: 199 Hot stream inlet: 570 Hot stream outlet: 230	Cold stream pressure: 25 Hot stream pressure: 25
Heat Exchanger Three	MHeatX	Cold stream inlet: 200 Cold stream outlet: 223 Hot stream inlet: 977 Hot stream outlet: 200	Cold stream pressure: 25 Hot stream pressure: 1
Heat Exchanger Four	MHeatX	Cold stream inlet: 25 Cold stream outlet: 600 Hot stream inlet: 1092 Hot stream outlet: 977	Cold stream pressure: 1 Hot stream pressure: 1
Heat Exchanger Five	MHeatX	Cold stream inlet: 25 Cold stream outlet: 600 Hot stream inlet: 843 Hot stream outlet: 79	Cold stream pressure: 1 Hot stream pressure: 1
Pump	Pump efficiency: 83 %	Inlet temperature: 20 Outlet temperature: 20	Inlet pressure: 1 Outlet pressure: 25
Compressor	Isentropic efficiency: 83 %	Inlet temperature: 25 Outlet temperature: 316	Inlet pressure: 1 Outlet Pressure: 25
PSA	Separator	25	25
Heater One	Heater	600	25

Table 11
Comparison of KPIs for SE-SMR-CLC with HX network, with previous processes.

Process	H_2 purity (%)	CO_2 capture rate (%)	Thermal efficiency (%)	Exergy efficiency *via* Eq. (12) (%)	Exergy efficiency *via* Eq. (16) (%)	Exergy destruction (kW)
SE-SMR- CLC with HX network	99.99	100	77.02	72.43	76.31	16,332.27
SE-SMR-CLC	99.99	100	76.99	67.68	70.48	22,007.67
SE-SMR-PCC	99.99	96.04	71.97	64.67	69.21	24,001.86

Table 12
Exergy destruction and exergy efficiency of individual processing units in the SE-SMR-CLC with HX network.

Processing units	Exergy efficiency (%)	Exergy destruction (kW)	Contribution to exergy destruction (%)
Fuel Reactor	97.98	3955.97	24.22
CND1	94.98	3111.46	19.05
HX2 (B19)	95.69	2873.25	17.59
Reformer	97.72	1767.31	10.82
Mixer 1 (B5)	97.88	1599.11	9.79
HX5	80.94	1065.83	6.53
Heater	99.48	399.61	2.45
CND2	80.50	379.74	2.33
HX4 (B2)	99.05	277.71	1.70
Mixer 3	96.73	215.64	1.32
HX1 (B21)	99.67	193.49	1.18
Air Reactor	99.90	175.84	1.07
HX3 (B17)	97.96	159.44	0.98
Compressor(B12)	99.83	88.49	0.54
Calciner	99.65	63.99	0.39
OSA	99.99	2.42	0.01
Pump (B6)	99.36	1.77	0.01
Mixer 2	99.99	1.09	0.01

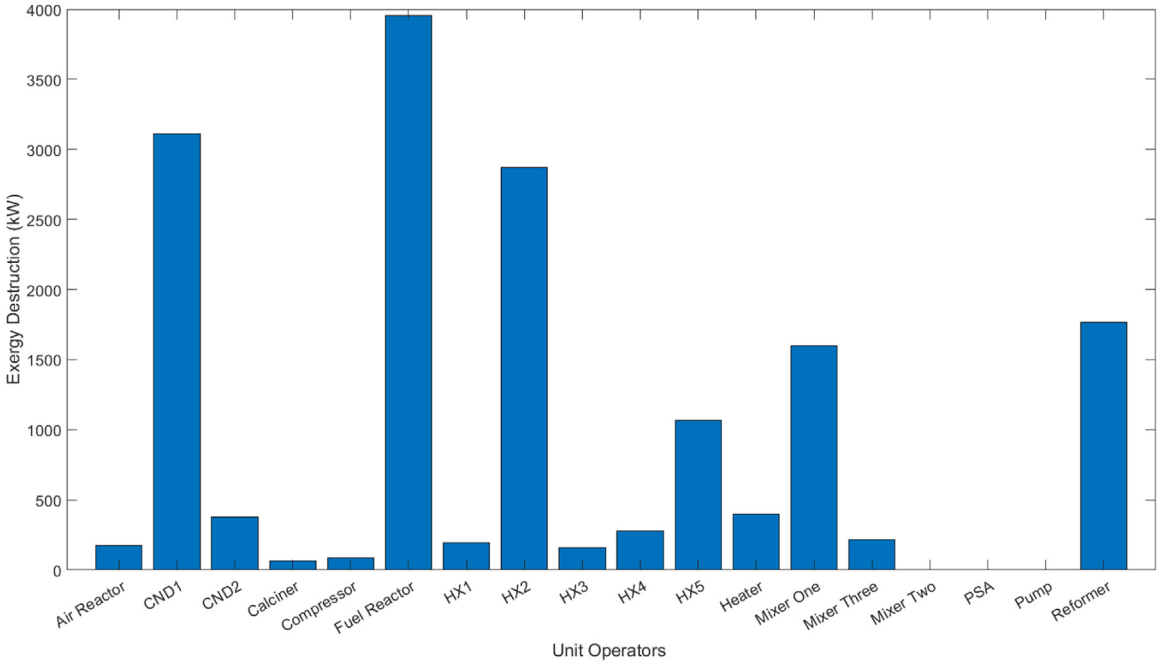

Fig. 12. Comparison of exergy destruction of individual processing units in the SE-SMR-CLC process.

Table 13
Exergy efficiency and destruction of SE-SMR-CLC process at different H_2 concentrations in the fuel reactor.

Process	Exergy efficiency *via* Eq. (16) (%)	Exergy destruction (kW)
SE-SMR-CLC (0 %)	76.31	16,332.27
SE-SMR-CLC (1 %)	76.74	15,765.57
SE-SMR-CLC (5 %)	77.58	14,371.54
SE-SMR-CLC (10 %)	77.02	14,026.56

tion in both the fuel and air reactor temperatures, providing a more efficient combustion process. After 5 % H_2 recycling there is a reduced exergy efficiency. This is due to the increase in H_2O that is generated due to the combustion of H_2. An increase of water vapour within the fuel reactor inhibits the reduction of Fe_2O_3 by blocking the active sites (Spreitzer and Schenk, 2019). As well as the cooling of H_2O involves a high exergy destruction due to the change in the chemical exergy value when H_2O is in a gaseous (9.5 kJ mol^{-1}) and liquid (0.9 kJ mol^{-1}) state. Further analysis is required to assess the impact of H_2 recycling on the overall costs, especially as this impacts the overall hydrogen production yield.

The conceptual process configuration presented in this work offers a high CO_2 capture rate due to the combined use of heat integration, calcium looping and CLC. The baseline case although is competitive with literature cases, has a reduced exergy efficiency due to the poor efficiency of the combustion system with PCC, the increased energy input required for the PCC system significantly reduces the exergy efficiency of the process. Integrating CLC into the process improves the combustion efficiency by developing a cyclic combustion process.

As well as changing the combustion system designing an efficient HX network is key in improving the exergy efficiency of the process. The recycling of H_2 to be used as the reducing agent offers a slight increase in exergy efficiency. The optimised process offers a higher thermodynamic performance in comparison to conventional SMR. Simultaneous CO_2 capture and H_2 production can be done in an energy-efficient manner by integrating the CCS technology within the process. For example, by integrating a calcium looping system within the reformer, the CaO interaction provides heat whilst capturing the CO_2, meaning there is a reduction in the reformer temperature in comparison to the SMR process. This consequently reduces the contribution of the reformer to the total exergy destruction of the process.

Further investigation is required to assess how this process may evolve over time, including the long-term performance of CaO sorbents and various types of oxygen carriers, and the ways these would impact the overall exergy efficiency of the process. Furthermore, within the development of this novel process configuration, further optimisation is required with respect to the operating conditions. Future work will look to incorporate machine learning to determine the optimal operating conditions for the process.

4. Conclusion and future work

Blue hydrogen production will play a part in the decarbonisation of multiple industries such as steel, shipping and refineries. Ensuring the deployment of blue hydrogen production is of paramount importance to ensure it makes an immediate and significant impact with respect to net-zero. Assessment of the integration of these CCS technologies is of paramount importance, specifically, the exergy analysis of processes can provide the true thermodynamic efficiencies of a process. An exergy analysis was performed on an SE-SMR process with an amine scrubbing unit as a PCC system with a high CO_2 capture rate (96.04 %), and a comparable exergy efficiency (69.21 %). A breakdown of the exergy destruction highlights that the exergy destruction occurs within the combustion and PCC systems. The development of an HX network and a CLC unit to replace the previous units yields an improved CO_2 capture rate, and exergy efficiency (76.31 %). Further assessment revealed that integration of a 5 % (molar) of produced H_2 from the process results in an improved exergy efficiency (77.58 %). Due to the cyclic nature of CLC and calcium looping, it is important to assess the materials' performance over time and therefore, future work should focus on the development of a dynamic model to shed light on how the exergy efficiency could be impacted over time. The recycling of the H_2 must be further assessed *via* a techno-economic analysis of this process to fully understand the viability of the proposed conceptual design at scale.

Data availability statement

All the generated data in this work has been presented and integrated within the paper in form of tabulated data.

Declaration of competing interest

The authors declare that they have no known competing financial interests or personal relationships that could have appeared to influence the work reported in this paper.

Acknowledgements

The research presented in this work has received financial support from the UK Engineering and Physical Sciences Research Council (EPSRC) through the project "*Multiphysics and multiscale modelling for safe and feasible CO_2 capture and storage* - EP/T033940/1", as well as *via* the EPSRC Doctoral Training Partnerships (DTP) award, EP/T518116/1 (project reference: 2688399). The authors would also like to acknowledge the UKCCSRC ECR Collaboration Fund 2022 (call 4) for the financial support of the collaboration between the researchers in this work.

References

Antzara, A., Heracleous, E., Bukur, D.B., Lemonidou, A.A., 2015. Thermodynamic analysis of hydrogen production via chemical looping steam methane reforming coupled with in situ CO_2 capture. Int. J. Greenh. Gas Control 32, 115–128. doi:10.1016/j.ijggc.2014.11.010.

Chew, Y.E., Xin, A., Cheng, H., Chun, A., Loy, M., Shen How, B., Andiappan, V, 2023. Beyond the colours of hydrogen: opportunities for process systems engineering in hydrogen economy. Process Integr. Optim. Sustain. 7, 941–950. doi:10.1007/s41660-023-00324-z.

Davies, W.G., Babamohammadi, S., Yang, Y., Soltani, S.M., 2023. *The rise of the machines:* a state-of-the-art technical review on process modelling and machine learning within hydrogen production with carbon capture. Gas Sci. Eng. 118, 205104. doi:10.1016/j.jgsce.2023.205104.

Cranfield University the Gas Technology Institute Doosan Babcock (2019). *Phase 1 SBRI Hydrogen Supply Competition Bulk Hydrogen Production by Sorbent Enhanced Steam Reforming (HyPER) Project Executive Summary*.

DESNZ and BEIS (2021a), *Net Zero Strategy: Build Back Greener*, UK, https://www.gov.uk/government/publications/net-zero-strategy.

DESNZ and BEIS (2021b), *UK Hydrogen Strategy*, UK, https://www.gov.uk/government/publications/uk-hydrogen-strategy

Environment Agency (2023), *Emerging techniques for hydrogen production with carbon capture,* UK, https://www.gov.uk/government/publications/emerging-techniques-for-hydrogen-production-with-carbon-capture/emerging-techniques-for-hydrogen-production-with-carbon-capture

Fan, J., Zhu, L., Jiang, P., Li, L., Liu, H., 2016. Comparative exergy analysis of chemical looping combustion thermally coupled and conventional steam methane reforming for hydrogen production. J. Clean. Prod. 131, 247–258. doi:10.1016/J.JCLEPRO.2016.05.040.

Fu, Z., Lu, L., Zhang, C., Xu, Q., Zhang, X., Gao, Z., Li, J., 2023. Fuel cell and hydrogen in maritime application: a review on aspects of technology, cost and regulations. Sustain. Energy Technol. Assess. 57, 103181. doi:10.1016/j.seta.2023.103181.

García, R., Gil, M.V., Rubiera, F., Chen, D., Pevida, C., 2020. Renewable hydrogen production from biogas by sorption enhanced steam reforming (SESR): a parametric study. Energy 218, 119491. doi:10.1016/j.energy.2020.119491.

George, J.F., Müller, V.P., Winkler, J., Ragwitz, M., 2022. Is blue hydrogen a bridging technology?—The limits of a CO_2 price and the role of state-induced price components for green hydrogen production in Germany. Energy Policy 167. doi:10.1016/j.enpol.2022.113072.

Hajjaji, N., Pons, M.N., Houas, A., Renaudin, V., 2012. Exergy analysis: an efficient tool for understanding and improving hydrogen production via the steam methane reforming process. Energy Policy 42, 392–399. doi:10.1016/j.enpol.2011.12.003.

https://www.theguardian.com/environment/2023/aug/28/crazy-off-the-charts-records-has-humanity-finally-broken-the-climate. Date Accessed (28/08/23).

IEA (2021), *Net Zero by 2050*, IEA, Paris, https://www.iea.org/reports/net-zero-by-2050, License: CC BY 4.0

IEA (2022), *Global Hydrogen Review 2022, Global Hydrogen Review 2022*. www.iea.org//reports/global-hydrogen-review-2022, License: CC BY 4.0

Ishaq, H., Dincer, I., Crawford, C., 2022. A review on hydrogen production and utilization: challenges and opportunities. Int. J. Hydrogen Energy 47 (62), 26238–26264. doi:10.1016/j.ijhydene.2021.11.149.

Johnsen, K., Ryu, H.J., Grace, J.R., Lim, C.J., 2006. Sorption-enhanced steam reforming of methane in a fluidized bed reactor with dolomite as CO_2-acceptor. Chem. Eng. Sci. 61, 1195–1202. doi:10.1016/j.ces.2005.08.022.

Kwak, N.-S., Lee, J.H., Lee, I.Y., Jang, K.R., Shim, J.-G., 2012. A study of the CO_2 capture pilot plant by amine absorption. Energy 47, 41–46. doi:10.1016/j.energy.2012.07.016.

Marocco, P., Gandiglio, M., Audisio, D., Santarelli, M., 2023. Assessment of the role of hydrogen to produce high-temperature heat in the steel industry. J. Clean. Prod. 388, 135969. doi:10.1016/j.jclepro.2023.135969.

Masoudi Soltani, S., Lahiri, A., Bahzad, H., Clough, P., Gorbounov, M., Yan, Y, 2021. Sorption-enhanced steam methane reforming for combined CO_2 capture and hydrogen production: a state-of-the-art review. Carbon Capture Sci. Technol. 1, 100003. doi:10.1016/j.ccst.2021.100003.

Mohamadi-Baghmolaei, M., Hajizadeh, A., Zahedizadeh, P., Azin, R., Zendehboudi, S., 2021. Evaluation of hybridized performance of amine scrubbing plant based on exergy, energy, environmental, and economic prospects: a gas sweetening plant case study. Energy 214, 118715. doi:10.1016/J.ENERGY.2020.118715.

Simpson, A.P., Lutz, A.E., 2007. Exergy analysis of hydrogen production via steam methane reforming. Int. J. Hydrogen Energy 32 (18), 4811–4820. doi:10.1016/j.ijhydene.2007.08.025.

Singh, S., Jain, S., Ps, V., Tiwari, A.K., Nouni, M.R., Pandey, J.K., Goel, S., 2015. Hydrogen: a sustainable fuel for future of the transport sector. Renew. Sustain. Energy Rev. 51, 623–633. doi:10.1016/j.rser.2015.06.040.

Soltani, S.M., Fennell, P.S., Mac Dowell, N., 2017. A parametric study of CO_2 capture from gas-fired power plants using monoethanolamine (MEA). Int. J. Greenh. Gas Control 63, 321–328. doi:10.1016/j.ijggc.2017.06.001.

Spreitzer, D., Schenk, J., 2019. Reduction of iron oxides with hydrogen—A review. Steel Res. Int. 90 (10). doi:10.1002/SRIN.201900108.

Szargut, J., 1989. Chemical exergies of the elements. Appl. Energy 32 (4), 269–286. doi:10.1016/0306-2619(89)90016-0.

Tzanetis, K.F., Martavaltzi, C.S., Lemonidou, A.A., 2012. Comparative exergy analysis of sorption enhanced and conventional methane steam reforming. Int. J. Hydrogen Energy 37 (21), 16308–16320. doi:10.1016/J.IJHYDENE.2012.02.191.

Wang, X., Lo, K., 2021. Just transition: a conceptual review. Energy Res. Soc. Sci. 82, 102291. doi:10.1016/j.erss.2021.102291.

Yan, Y., Manovic, V., Anthony, E.J., & Clough, P.T. (2020a). Techno-economic analysis of low-carbon hydrogen production by sorption enhanced steam methane reforming (SE-SMR) processes. *Energy Convers. Manag.*, 226. https://doi.org/10.1016/j.enconman.2020.113530

Yan, Y., Thanganadar, D., Clough, P.T., Mukherjee, S., Patchigolla, K., Manovic, V., Anthony, E.J., 2020b. Process simulations of blue hydrogen production by upgraded sorption enhanced steam methane reforming (SE-SMR) processes. Energy Convers. Manag. 222. doi:10.1016/j.enconman.2020.113144.